Ionics (2017) 23:2229–2240
DOI 10.1007/s11581-017-2167-x

REVIEW

Chemical and physical characterizations of the $n = 1$ Ruddlesden–Popper phases: $Nd_{2-y}Sr_yNi_{1-x}Co_xO_{4\pm\delta}$ ($y = 1$ and $0.1 \leq x \leq 0.9$)

Hanèn Chaker[1] · **I. Raies**[1] · **A. Chouket**[1] · **T. Roisnel**[2] · **R. Ben Hassen**[1]

Received: 6 March 2017 / Revised: 20 May 2017 / Accepted: 22 May 2017 / Published online: 15 June 2017

Abstract The structural stability and physical properties of $NdSrNi_{1-x}Co_xO_{4\pm\delta}$ ($0.1 \leq x \leq 0.9$) mixed oxides, elaborated by conventional sol–gel process, have been investigated and obtained results show that substitution of nickel by cobalt at $x = 0.5$ enhances conductivity at room temperature; $\sigma = 17.24\ \Omega^{-1}\ cm^{-1}$ coinciding with minimum activation energy ($E_a = 0.05$ eV). Rietveld refinements of X-ray powder diffraction patterns at room temperature indicate that all compositions crystallize in a tetragonal system with I4/mmm space group and exhibit K_2NiF_4-type structure. Variations of a and c parameters display various behavior with increasing cobalt content. Changes in cell parameters are discussed in terms of crystal field theory. In addition, transition metal oxidation state is investigated on the basis of the Brown bond valence calculation. The deduced Global Instability Index (GII) value decreases when cobalt substance increases, indicating that the structure becomes more stable once cobalt is introduced. Oxygen stoichiometry of these compounds was determined from thermogravimetric analyses (TGA) followed by reduction in 5% H_2 in N_2 gas. Conductivity of $NdSrNi_{1-x}Co_xO_{4\pm\delta}$ ($0.1 \leq x \leq 0.9$) oxides was measured by an ac four-probe method. Oxygen vacancies are the possible ionic charge carriers. Specimens exhibit a semiconducting behavior in the whole range of temperature. The electrical transport mechanism agrees with an adiabatic small polaron hopping (ASPH) model.

Keywords Functional oxides · Sol–gel preparation · Rietveld analysis · K_2NiF_4-type structure · Thermogravimetric analysis · Electrical properties

Introduction

The Ruddlesden–Popper series displaying the K_2NiF_4-type structure are the central focus of researchers especially chemists and physicists as they present a wide range of chemical and physical properties. Indeed, they permeate diverse fields as superconductivity [1], magneto resistance [2, 3], catalysis [4], and mixed ionic–electronic conductivity [5].

In particular, several authors have been attracted by the possible application of Ln_2MO_4 compounds (Ln = rare earth; M = Co, Ni) such as oxygen membrane or electrode in solid oxide fuel cells (SOFCs) in addition to solid oxide electrolysis cell (SOEC) devices [6–8]. Furthermore, doping these compounds with alkaline earth and transition metal can modulate not only the oxygen content in the system but also the average oxidation state of the transition metal ion [9, 10].

The majority of investigations are devoted to lanthanum compounds, only few were interested in neodymium rare earth. In fact, Moritomo et al. had explored $La_{2-x}Sr_xCoO_4$ ($0.4 \leq x \leq 1.0$) solid solution with a mixed valence of cobalt ion (Co^{2+}/Co^{3+}) and found steep decreases in electrical resistivity with an increase in the amount of Sr beyond the value 0.7 [11, 12]. Next to these

✉ Hanèn Chaker
hanen_chaker@yahoo.fr

[1] Unité de Chimie des Matériaux et de l'Environnement, UR11ES25, ISSBAT, Université de Tunis El Manar, 9 Avenue Dr. Zoheir Safi, 1006 Tunis, Tunisia

[2] Institut des Sciences Chimiques de Rennes, UMR CNRS 6226, Université de Rennes 1, Campus de Beaulieu, 35042 Rennes Cedex, France

Table 1 Lattice parameters, volume, and tolerance factor for all compositions

Composition (x)	$a = b$ (Å)	c (Å)	Volume (Å^3)	Tolerance factor
0.0	3.7963 (1)	12.2971 (2)	177.224 (4)	0.951
0.1	3.7875 (2)	12.3456 (4)	177.099 (2)	0.945
0.3	3.7834 (9)	12.3528 (6)	176.819 (4)	0.937
0.5	3.7824 (3)	12.3315 (2)	176.421 (2)	0.928
0.7	3.7804 (4)	12.2798 (8)	175.495 (3)	0.920
0.9	3.7799 (1)	12.2652 (5)	175.240 (1)	0.912

attempts, Kharton et al. reported that the conductivity of layered $La_2Ni_{1-x}Co_xO_{4+\delta}$ is predominantly p-type electronic within the stability domain (x = 0.1–0.2) phase and occurs via small polaron mechanism, which is indicated by temperature-activated hole mobility and $p(O_2)$ dependencies of electrical properties [13].

Over the last decade, great interest has been paid to neodymium oxides $Nd_{2-x}Sr_xCoO_4$ with the K_2NiF_4-type structure for the discovery of magneto resistance and superconductivity [14, 15]. D. Grandjean et al. [16] have studied the effect of cobalt substitution for copper in the parent compound $NdSrCoO_4$, and highlighted that this doping produces quite dissimilar oxide coordination environments for the dopant and copper ion which may change spin state.

A previous study performed by H. Chaker et al. [17] focused on the effect of copper substitution in $NdSrNiO_4$ which showed a metal-semiconductor transition at ~190 K [18]. Structural and conductivity results for the composition $NdSrNi_{0.8}Cu_{0.2}O_4$ reveal that this phase is a possible candidate for integrated devices like, for example, bottom electrode in parallel plate ferroelectric capacitors. At the second stage of this study, we used this electrode to epitaxial growth for a functional oxide, namely the Aurivillius phase ferroelectric [19].

As we got more and more interested in our lab in mixed oxides based on neodymium, erbium, and dysprosium rare earths, we have already reported in previous works the obtained results after substitution of nickel for copper and chromium [20–26].

Within this framework, our present work is an extension to our previous studies on neodymium nickelate-based mixed oxide. It aims to investigate the effect of cobalt incorporation in the parent compound $NdSrNiO_4$ on the structural features and the ability to accommodate oxygen non-stoichiometry. We suspect that these new functional K_2NiF_4-type oxides should form a very interesting family of materials: their physical properties and the possibility to combine them with a ferroelectric oxide in heterostructures by epitaxy open a way for fabricating innovating and high-performance components for applications in microelectronic and as electrode in SOFCs operating at intermediate temperatures.

For this reason, we have synthesized new compounds in the $NdSrNi_{1-x}Co_xO_{4\pm\delta}$ ($0.1 \le x \le 0.9$) system by sol–gel method. We report here some preliminary results of powder X-ray diffraction, thermogravimetric analysis, bond valence calculation, and resistivity measurements.

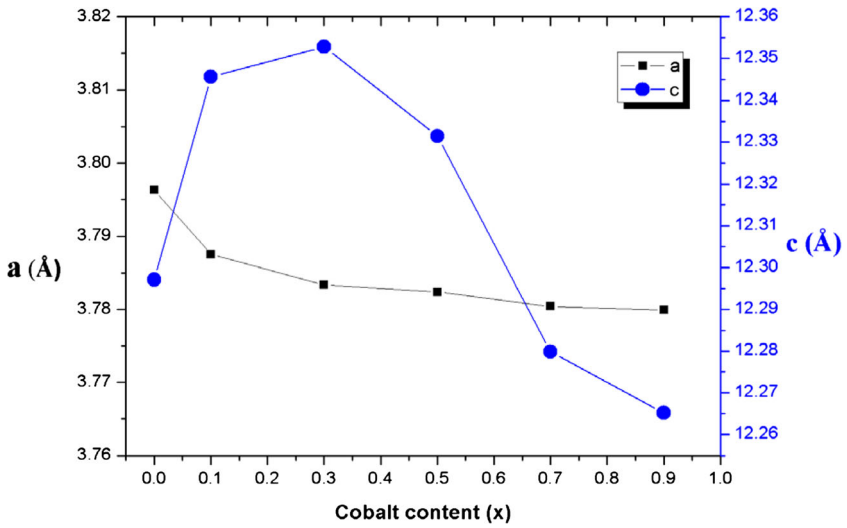

Fig. 1 Evolution of unit cell parameters with cobalt content (x). Data for x = 0 are taken from literature

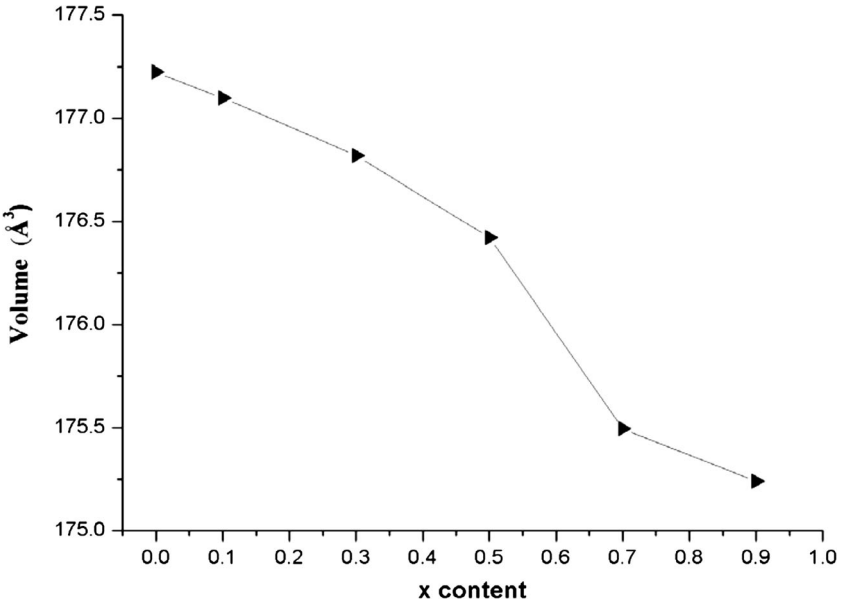

Fig. 2 Evolution of unit cell volume with x in the $NdSrNi_{1-x}Co_xO_{4\pm\delta}$ ($0.0 \le x \le 0.9$) solid solution

Materials and methods

Polycrystalline samples with particular compositions (x = 0.1, 0.3, 0.5, 0.7 and 0.9) have been synthesized in the solid solutions $NdSrNi_{1-x}Co_xO_{4\pm\delta}$ from powders Nd_2O_3 (Aldrich, 99.99%), $SrCO_3$, NiO, and Co_3O_4 (Aldrich, 99.99%) by the sol–gel method in the desired mole ratio in the reaction:

$$1\Big/2Nd_2O_3+SrCO_3+(1-X)NiO+x \times 1\Big/3Co_3O_4\rightarrow NdSrNi_{1-x}Co_xO_{4\pm\delta}+CO_2$$

Neodimium oxide, strontium carbonate, nickel, and cobalt oxides were initially independently dissolved in a minimum quantity of concentrated chlorid acid with magnetic stirring. After intimate mixture of these solutions with distilled water, citric acid $C_6H_8O_7{\cdot}H_2O$ and ethylene glycol $C_2H_6O_2$ were then added. The obtained sol was left on a hot plate with constant stirring for approximately 5 h at 80 °C until it gelled and changed the color from transparent purple to green. After that, the formed pale green gel was treated by further heating, first at 200 °C for approximately 24 h then at 450 °C in a muffle furnace. The resulting powder was ground before it was returned to the furnace in air at 600 °C for 48 h. The calcined mixtures were subsequently pressed into pellets (13-mm diameter and 2-mm thickness under 10 t/cm^2) and annealed in a tube furnace at 1150 °C in a flow of oxygen and cooled to room temperature at a rate of 100°/h for 3 days with intermediate regrinding and repelleting until no further reaction was established by powder X-ray diffraction.

Powder X-ray diffraction data for the six samples (x = 0.1, 0.3, 0.5, 0.7 and 0.9) were collected at room temperature using a Bruker D8 Advance, with a monochromatic CuKα_1 radiation (λ = 1.54056 Å). Data were

Table 2 The refined composition of samples from EDX analysis

x composition	Element	Atomic %	Refined composition	Nominal composition
0.1	O	59.46	4.163	4
	Co	1.42	0.099	0.1
	Ni	12.53	0.877	0.9
	Sr	14.03	0.982	1
	Nd	12.56	0.879	1
0.3	O	58.70	4.109	4
	Co	4.42	0.309	0.3
	Ni	9.71	0.679	0.7
	Sr	13.72	0.960	1
	Nd	13.45	0.941	1
0.5	O	57.85	4.049	4
	Co	6.71	0.469	0.5
	Ni	6.85	0.479	0.5
	Sr	14.1	0.987	1
	Nd	14.49	1.014	1
0.7	O	58.42	4.089	4
	Co	9.85	0.689	0.7
	Ni	4.14	0.289	0.3
	Sr	14.57	1.019	1
	Nd	13.02	0.911	1
0.9	O	60.28	4.219	4
	Co	11.71	0.819	0.9
	Ni	1.28	0.089	0.1
	Sr	14.14	0.989	1
	Nd	12.59	0.881	1

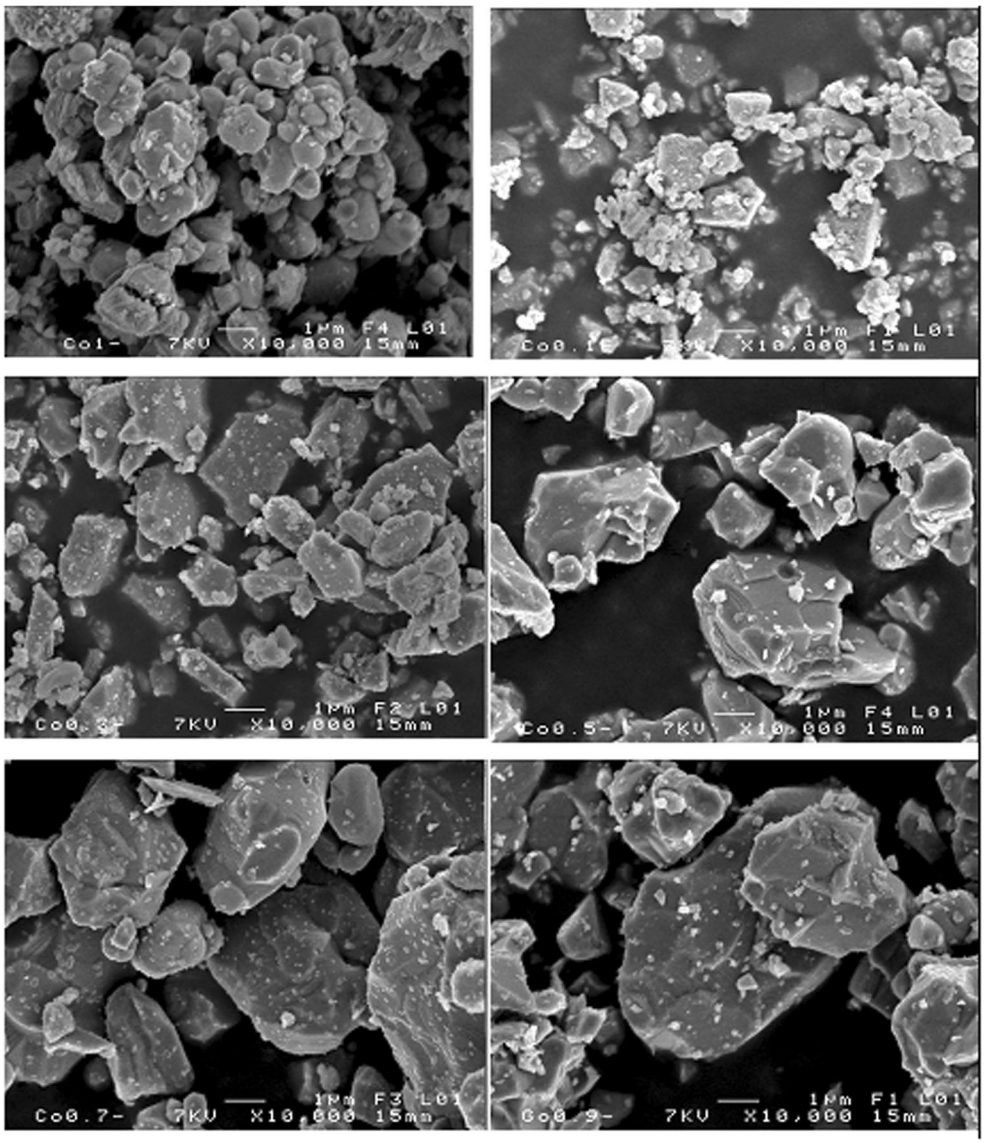

Fig. 3 SEM micrographs of the six samples in the same scale

collected with a 0.0105° step 2θ width and ≈ 2-s counting time per point over a 2θ range from 10 to 120°. The whole pattern profile refinements were carried out with the FullProf program [27].

The morphological features and grain size of the particles were studied by scanning electron microscopy (SEM) on a JSM-6400 apparatus working at 20 kV at room temperature. For this reason, the samples were ground, deposited, and then metalized. Compositional analyses were performed by recording the energy dispersive X-ray analysis (EDX).

The total oxygen content of the samples was determined by hydrogen reduction in a TGDTA 92-SETARAM thermogravimetric analyzer (TGA). The material was heated in an alumina pan under flowing dried 5% H_2 in N_2 gas (1.5 l/h) from room temperature up to 1100 °C at a rate of 10 °C/min.

The temperature dependence of dc resistivity $\rho(T)$ was measured by the conventional four-probe method under high vacuum conditions using the van der Pauw method [28]. The latter was implemented through cooling down the samples from 390 to 20 K with a rate of 1 K/min using the Cryodyne Industries Refrigerator, model 22.

Results and discussion

Structural study

Departing from the superposition of the patterns of all prepared compositions in the $NdSrNi_{1-x}Co_xO_{4\pm\delta}$ ($0.1 \le x \le 0.9$) system, it is deduced that the corresponding compounds are structurally identical and no evidence for a

Table 3 Profile and structural parameters from Rietveld refinement for $NdSrNi_{0.5}Co_{0.5}O_{4-\delta}$

$NdSrNi_{0.5}Co_{0.5}O_{4-\delta}$						
I4/mmm; ($Z = 2$)						
$a = 3.7824$ (3) Å						
$c = 12.3315$ (2) Å,						
$V = 176.421$ (2) Å^3						
Density = 6.670 g/cm^3						
Atoms	W. P.	x	y	z	B_{iso} (Å^2)	Occupation
Nd/Sr	4e	0	0	0.3606 (8)	0.426 (9)	0.506/0.494
Ni/Co	2a	0	0	0	0.357 (7)	0.242/0.258
O1	4c	0	00.5	0	0.174 (8)	0.994
O2	4e	0	0	0.0.1679 (6)	0.509 (3)	1.00
R factors (%)						
$R_{Bragg} = 7.16$						
$R_F = 5.2$						
$R_p = 4.5$						
$R_{wp} = 6.1$						
$R_{exp} = 3.6$						
$\chi^2 = 2.66$						

structural phase transition was detected when varying the composition of the cobalt. In fact, auto-indexing of the whole pattern profile of the X-ray peaks for all compositions led to only one solution with all lines indexed and a good figure of merit. Profile analysis has been performed on the basis of a tetragonal system with space group I4/mmm. The peak shape was described by a pseudo-Voigt function (Thomson–Cox–Hasting (TCH)).

For each diffraction pattern, a zero-point shift and unit cell parameters were refined in addition to profile parameters. The background was fitted with a linear interpolation between 24 chosen points. The lattice parameters deduced from the whole pattern profile refinement ("pattern matching" mode in FullProf) of the X-ray data are presented in Table 1.

Figure 1 portrays the variation of the lattice parameters as a function of x in $NdSrNi_{1-x}Co_xO_{4\pm\delta}$ ($0.1 \le x \le 0.9$) compounds (results for $x = 0$ have been reported from a preceding research [17]). As it can be observed in this figure, the c parameter, at the first time, increases clearly with doping cobalt but subsequently,

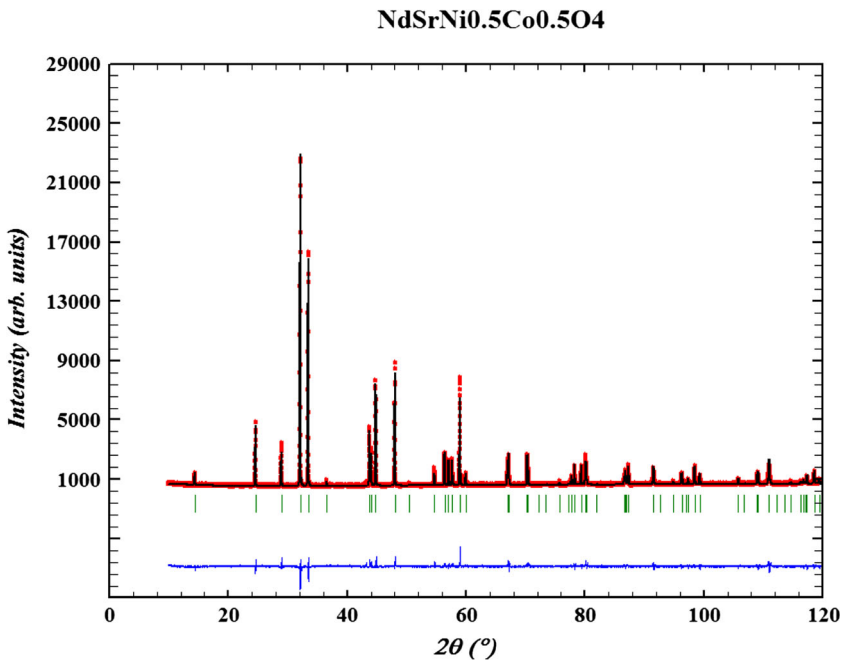

Fig. 4 Observed (*dotted*) and calculated (*solid*) *lines* of the final Rietveld refinement. The *lower line* is relative to the difference pattern ($Y_{obs} - Y_{cal}$), whereas *vertical tics* correspond to the 2θ Bragg positions

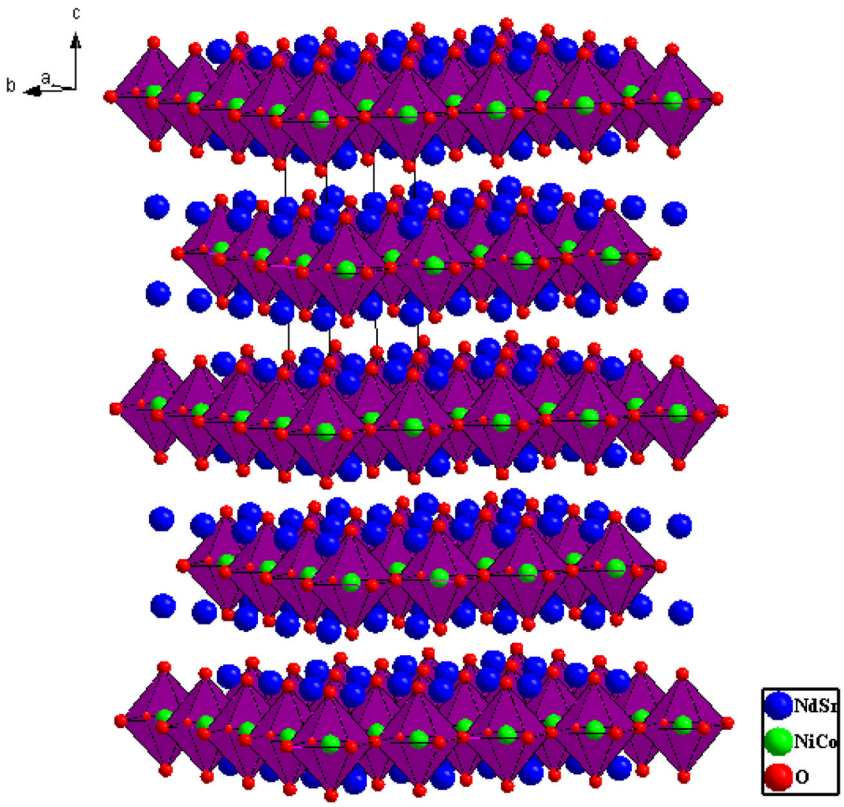

Fig. 5 Tetragonal K_2NiF_4-type structure of $NdSrNi_{1-x}Co_xO_{4\pm\delta}$ ($0.0 \le x \le 0.9$) compounds

it decreases remarkably. On the other side, a parameter decreases slightly then remains unchangeable.

To explain these evolutions, we need to take into account the Jahn–Teller effect in $(Ni/Co)O_6$ octahedron. In fact, the fractional substitution of Ni^{3+} adopting $t_{2g}^6 d_{x^2-y^2}^1 d_{z^2}^0$ configuration in the $NdSrNiO_4$ parent compound [17] by Co^{2+}, which usually exhibits $t_{2g}^6 d_{z^2}^1 d_{x^2-y^2}^0$ configuration in low spin state as declared in tetragonal symmetry, causes an increase only of c parameter owing to the increase in electron quantity in the $\vec{c}$ direction. Moreover, the slight decrease in a parameter is due to the deficiency of one electron in $\vec{a}$ and $\vec{b}$ directions compared to Ni^{3+} (change in e_g^1 configuration: d_{z^2} orbital is occupied instead of $d_{x^2-y^2}$).

Furthermore, for a higher percentage of cobalt than nickel, parameter c decreases dramatically. This results from the fact that Co^{2+} (0.65 Å) oxidizes to smaller Co^{3+} (0.545 Å) ion for low spin state in sixfold coordination [29]. This finding is in good agreement with the statement of (+III) oxidation for nickel and the mixed valence (+II/+III) for cobalt. The unit cell volume, shown in Fig. 2, decreases with x in the series $NdSrNi_{1-x}Co_xO_{4\pm\delta}$ ($0.0 \le x \le 0.9$), but the reduction rate proves to be significant for $x \ge 0.5$.

In order to ascertain the cobalt content in the prepared materials, semiquantitative analysis using EDX was carried

Table 4 Inter-atomic distances (Ni/Co)–O and (Nd/Sr)–O for $x = 0.5$

Cobalt content		$x = 0.5$
Ni/Co—O (1) Å	×4	1.8922 (1)
Ni/Co—O (2) Å	×2	2.0705 (3)
Nd/Sr—O (1) Å	×4	2.5558 (2)
Nd/Sr—O (2) Å	×1	2.3773 (4)
Nd/Sr—O (2) Å	×4	2.6991 (1)

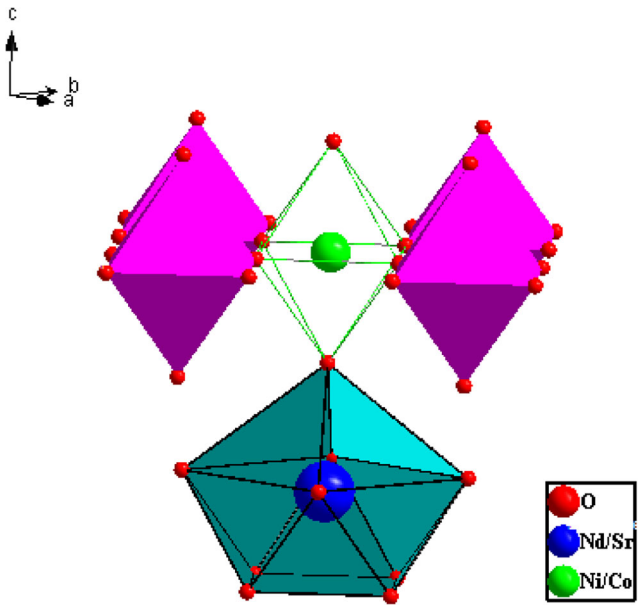

Fig. 6 (Nd/Sr) and (Ni/Co) environments for $NdSrNi_{0.5}Co_{0.5}O_{4-\delta}$

Table 5 Cobalt bond valence sum and Global Instability Index result

X	0.1	0.3	0.5	0.7	0.9
BVS	2.426	2.581	2.616	2.649	2.716
GII	0.489	0.401	0.397	0.387	0.382

BVS bond valence sum, *GII* Global Instability Index

out. These measurements prove the presence of all the chemical elements with their stoichiometric proportions. The results of the analysis are largely summarized in Table 2.

A general tendency was observed through SEM. In fact, the particle size extended and the porosity, as a matter of fact, diminished when we have progressively introduced cobalt instead of nickel. Consequently, the powder became more and more dense and crystallized with homogenous distribution. Figure 3 displays SEM micrographs of the six samples with the same scale.

Identifying tolerance factor (t) for layered oxide having K_2NiF_4 structure is established by $t = \frac{A-O}{\sqrt{2}(B-O)}$, where A–O and B–O are the metal–oxygen bond lengths of A-site and B-site cation, respectively. Referring to Goldschmidt [30], K_2NiF_4-type structure can be formed when ($0.85 < t < 1.05$). On this basis, the tolerance factor was calculated using tabulated values of ionic radii [29]. These are presented in Table 1 for $NdSrNi_{1-x}Co_xO_{4\pm\delta}$ ($0.0 \le x \le 0.9$) phases. Within this context, the tolerance factor values of these materials reside in the range $0.912 \le t \le 0.945$ for which the tetragonal distortion is favored [31].

The structural refinement of each composition in $NdSrNi_{1-x}Co_xO_{4\pm\delta}$ family was performed in the tetragonal system (I4/mmm space group) beginning with atomic positions taken from $NdSrNiO_4$ [32], which involves Nd^{3+} and Sr^{2+} ions that were disorganized over the ninefold coordinate 4e sites with their ratio according to the nominal composition (Table 2). The Ni and Co ions are situated at the 2a site, and the O1, O2 atoms are placed at (0, ½, 0) in site 4c and at (0, 0, z) in site 4e, respectively. At the final stage, good reliability factors are obtained as a result to refinement of all parameters, i.e., atomic coordinates, global atomic thermal displacement, and preferential orientation along the [001]. To illustrate these notions, the corresponding refined parameters of the $NdSrNi_{0.5}Co_{0.5}O_{4-\delta}$ compound are presented in Table 3 and the final fit is displayed in Fig. 4. Projection of the $NdSrNi_{0.5}Co_{0.5}O_{4-\delta}$ structure is portrayed in Fig. 5, and some corresponding inter-atomic distances are given in Table 4. Consequently, Ni/Co atoms shape a distorted octahedral where the axial (Ni/Co)–O1 band in the ab plane is shorter than the apical (Ni/Co)–O2 band along the c direction (Fig. 6). The coordination environments for strontium cation are highlighted also in Fig. 6.

Under this situation, metal–oxygen bonds are strained and the extension of these strains can be deduced using BVM (bond valence method) expressed by $S_{ij} = \exp[(R_0 - R_{ij}/B)]$, where R_0 and B (constant = 0.37) are the experimentally given parameters and R_{ij} is the bond length of the cation–anion pair. Referring to Brown [33], the sum of the bond valence around an ion has to be equal to the formal valence V_i of these ions $\left(V_i = \sum_{ij} S_{ij}\right)$. It is called VSR (valence sum rule). The deviation observed between these two values can be attributed to instabilities of the structure. The root mean square of

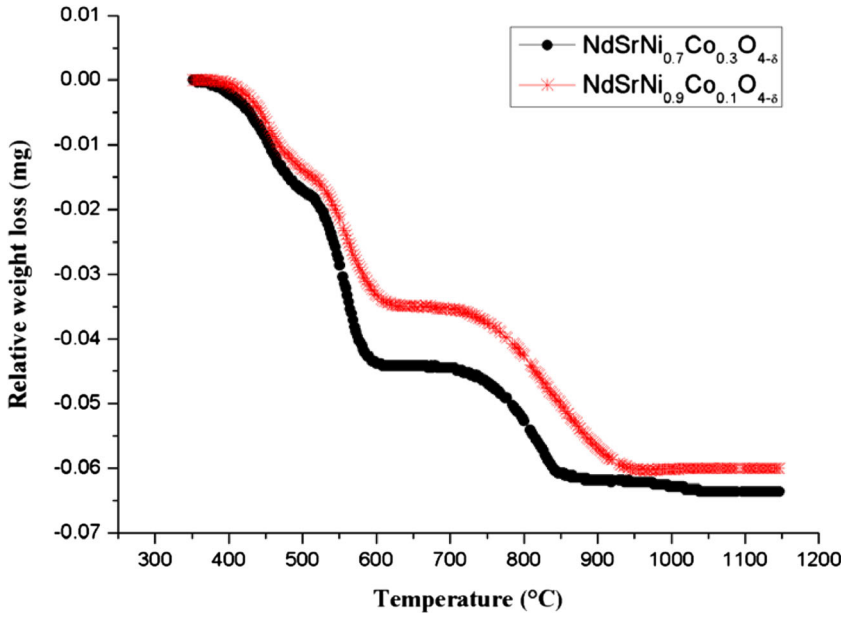

Fig. 7 The relative weight loss curve for $NdSrNi_{0.9}Co_{0.1}O_{4-\delta}$ and $NdSrNi_{0.7}Co_{0.3}O_{4-\delta}$

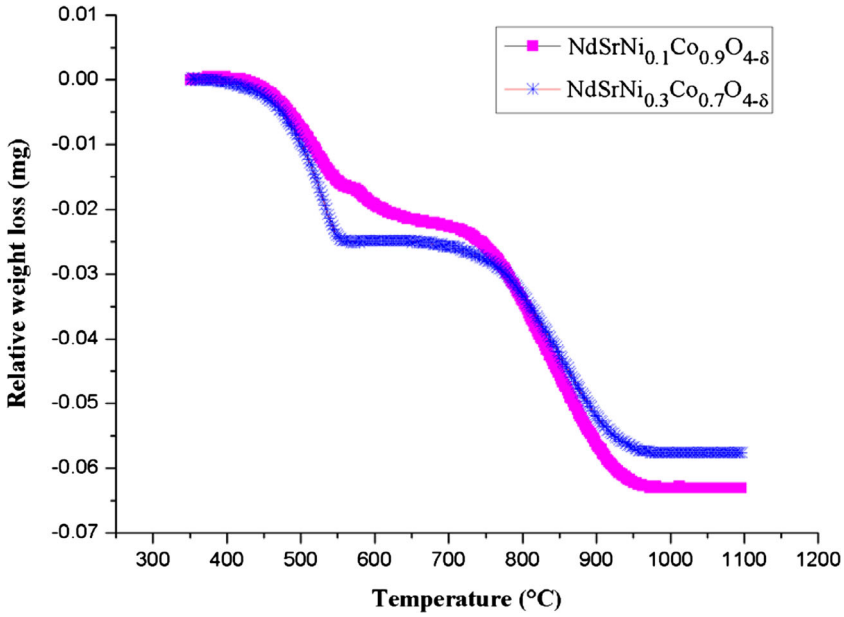

Fig. 8 The relative weight loss curve for $NdSrNi_{0.3}Co_{0.7}O_{4-\delta}$ and $NdSrNi_{0.1}Co_{0.9}O_{4-\delta}$

deviations for all atoms is named global instability index and expressed as [34] $GII = \sqrt{\frac{\sum_{i=1}^{N}\left\{\left(\sum_{j} S_{ij} - V_i\right)^2\right\}}{N}}$, where N is the number of atoms in the asymmetric unit. Sánchez-Andújar M. and Señarís-Rodríguez MA have investigated the Global Instability Index (GII) of K_2NiF_4-type $LnSrCoO_4$ (Ln = La, Nd, and Gd) [35] and demonstrated that GII decreases with the increase of the ionic radius of the rare earth ion and/or the doping level.

In the present work, the following R_0 values are used for subsequent calculations: 1.637 Å for Co^{3+}–O^{2-} bond, 1.686 Å for Ni^{3+}–O^{2-} bond, 2.105 Å for Nd^{3+}–O^{2-} bond, and 2.118 Å for Sr^{2+}–O^{2-} bond [36–38]. Computed bond valence sum by FullProf for cobalt atom concerning all compositions resting on Brown theory for oxygen deficiency on the $z = 0$ plane is recapitulated in Table 5. The GII of the $NdSrNi_{1-x}Co_xO_{4\pm\delta}$ ($0.1 \le x \le 0.9$) compounds illustrated also in Table 5 denotes that the crystal structure becomes more and more stable when we substitute nickel for cobalt.

Thermogravimetric analysis and oxygen stoichiometry determination

In order to investigate the variation in the oxygen deficiency as a function of cobalt proportion, we have performed thermogravimetric analysis in hydrogen/nitrogen atmosphere. A common aspect in the reduction curves for all compositions was the observation of a step-like behavior. These types of wide plateaus in the weight loss curves which appear throughout the reduction process are generally related to the stabilization of a number of phases with different oxygen stoichiometry [39]. Departing from the weight loss values, oxygen contents are deduced for all compositions taking into account Nd_2O_3, SrO, and metallic Ni and Co as final products. Figure 7 shows the relative weight loss curve for $NdSrNi_{0.9}Co_{0.1}O_{4-\delta}$ and $NdSrNi_{0.7}Co_{0.3}O_{4-\delta}$ which exhibit similar behavior. As it can be seen, the reduction phenomenon comprises three steps. The first process corresponds to the reduction of Ni^{3+} to Ni^{2+}. The second one stands for the reduction of Co^{3+} to Co^{2+}. The third plateau in this weight loss curve corresponds to reduction of Ni^{2+} and Co^{2+} into metallic nickel and cobalt without any distinction between them. Within the same framework, for both cases where $x = 0.7$ and $x = 0.9$, close results are recorded and presented in Fig. 8. In this specimen, the reduction phenomenon occurs only with two steps bringing about two plateaus. The first one for $\approx 400 \le T(C°) \le 550$, which stands for reduction of the majority of cobalt cation from Co^{3+} to Co^{2+} and minority of nickel from Ni^{3+} to Ni^{2+}. A second wide plateau is observed at $T(C°) \ge 750$ and corresponds to the complete reduction of cobalt and nickel ions to metal. Referring to Table 6, oxygen

Table 6 Oxygen content from TGA for all composition in $NdSrNi_{1-x}Co_xO_{4-\delta}$ solid solution

Cobalt content (x)	Oxygen content
0.0	3.995 (8) [17]
0.1	3.911 (3)
0.3	3.876 (7)
0.5	3.951 (1)
0.7	3.972 (2)
0.9	3.998 (1)

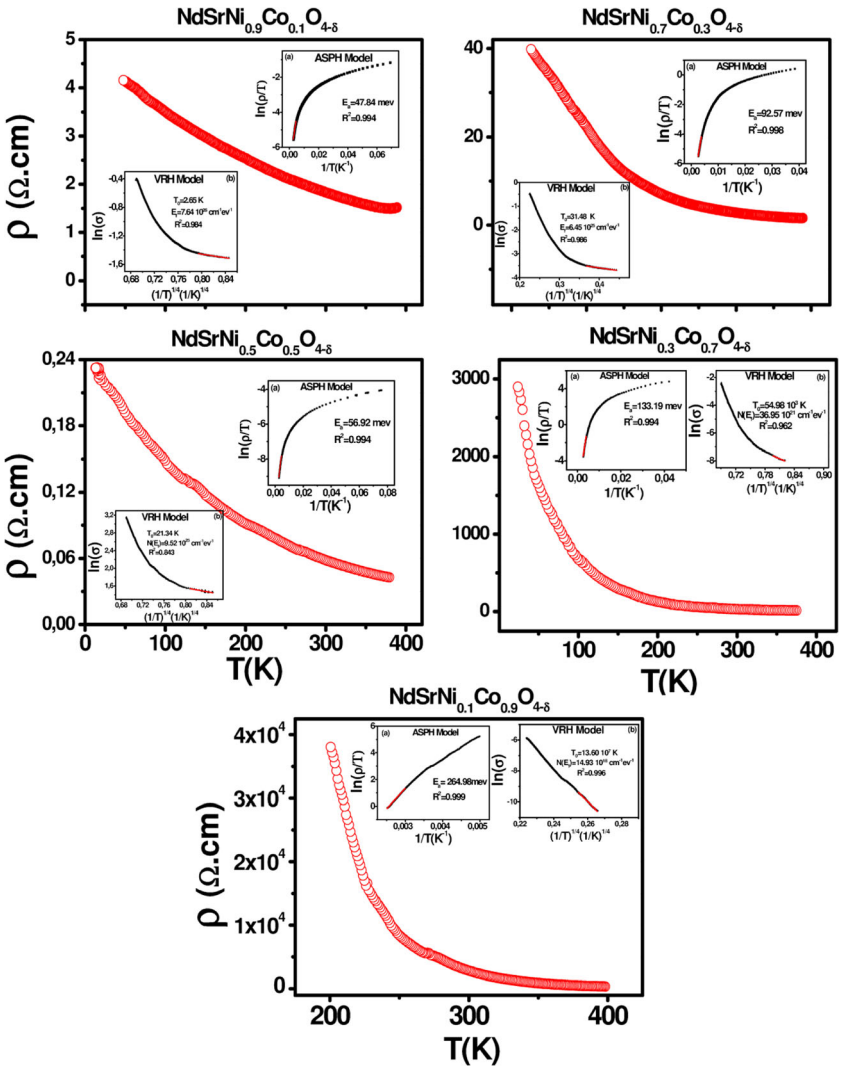

Fig. 9 Temperature dependence of ρ for x= 0.1, 0.3, 0.5, 0.7 and 0.9 in NdSrNi Co O. The inset (**a**) show ln(ρ /T) versus 1/T plots in the high-temperature region. full line is the fit to equation: ρ (T) = BT exp(Ea/kBT). The temperature dependence of the conductivity σ in scales of ln(σ) as a function of (1/T1/4) is also shown in the inset (**b**) with their fits (full lines) using the variable range hopping (VRH) model

content for the synthesized phases proves to be consistently under 4.00 atoms per formula unit and seems to be essentially dependent on the cobalt content. In fact, oxygen content diminishes up to $x = 0.3$ then rises with the increase of cobalt content. This behavior confirms the presence of Co^{3+} in compounds having a percentage of cobalt more or equal to 50%.

Electrical transport properties

The electrical resistivity measurements of $NdSrNi_{1-x}Co_xO_{4\pm\delta}$ ($0.1 \leq x \leq 0.9$) demonstrate that all the members of the solid solution are semiconducting between 20 and 390 K. In this common feature, the conductivity may be accounted for on the basis of two different models.

Firstly, Emin–Holstein theory of adiabatic small polaron hopping model (ASPH) [40], which is expressed as

$$\rho(T) = \mathrm{BT}\exp\left(E_a \Big/ k_B T\right) \tag{1}$$

where E_a is the activation energy for hopping conduction and B is the residual resistivity. Figure 9 portrays the corresponding results for the ASPH model, where the straight line is a fit to Eq. (1). The activation energy E_a is deduced from the fit of ln (ρ/T) versus $1/T$ curve.

Secondly, Mott et al. [41] have established the variable range hopping (VRH) mechanism, expressed by the following equation:

$$\rho(T) = \rho_0 \exp\left(T_0 \Big/ T\right)^{1/4} \tag{2}$$

where ρ_0 is considered as a constant which depends on electron–phonon interaction, though it is slightly affected by temperature [42]. The characteristic VRH temperature is noted $T_0 = 16.\alpha^3/k_\beta.N(E_F)$ where $N(E_F)$ is the density of states at the Fermi level. As a matter of fact, the T_0 value is calculated from the slope of the plot ln(σ) versus $T^{-1/4}$ (Fig. 9). Referring to [40], constant α was taken as 2.22 nm^{-1}. Table 7 illustrates

Table 7 Characteristic temperature T_0, density of state at the Fermi level $N(E_F)$, activation energy E_a, and correlation factors R for $NdSrNi_{1-x}Co_xO_{4-\delta}$ ($0.1 \le x \le 0.9$) using ASPH (Eq. 1) and VRH (Eq. 2) models

Composition in $NdSrNi_{1-x}Co_xO_{4-\delta}$	$x = 0.1$	$x = 0.3$	$x = 0.5$	$x = 0.7$	$x = 0.9$
ASPH model					
E_a (eV)	0.047	0.092	0.056	0.133	0.264
R^2	0.994	0.998	0.994	0.994	0.999
VRH model					
T_0 (K)	2.65	31.48	21.34	54.98×10^3	13.60×10^7
N (E_F) (eV^{-1} cm^{-3})	7.64×10^{26}	6.45×10^{25}	9.52×10^{25}	36.95×10^{21}	14.93×10^{18}
R^2	0.984	0.986	0.843	0.962	0.996

the computed values of T_0, $N(E_F)$, and E_a based on these two models. At this stage of analysis, it is worth noting that our results obtained for the semiconducting phase can be described quite well according to both models but the first one (ASPH) provides the best squared linear correlation coefficients (R^2). To conclude, we would assert that the transport behavior is dominated by the adiabatic small polaron hopping mechanism.

In this work and in related references [43–45], it is inferred that the obtained values of activation energy for $NdSrNi_{1-x}Co_xO_{4\pm\delta}$ (x = 0.1, 0.3, and 0.5) compounds (Table 7) are lower than that for $NdSrCoO_4$ [43]. Summing up these results, it can be concluded that after the incorporation of nickel and cobalt in the same site, we obtain a semiconductor material with conductivity in the range 0.3–17.24 Ω^{-1} cm^{-1} and low activation energy. The same result is found by several authors, for instance for the $NdSrNi_{0.5}Cr_{0.5}O_{4\pm\delta}$ compound, the σ_{RT} = 8.86 Ω^{-1} m^{-1}; E_a = 0.09 eV [25], for $Nd_{1.8}Sr_{0.2}Ni_{0.6}Cu_{0.4}O_{4\pm\delta}$ the $\sigma_{640°C}$ = 42.7 (3) S cm^{-1}; E_a = 0.07 eV [46] and for $NdSrNi_{0.8}Cu_{0.2}O_{4\pm\delta}$ the σ_{RT} = 1.13 Ω^{-1} cm^{-1}; E_a = 0.06 eV [17].

Based on the outcome of our investigation, it is possible to conclude that $NdSrNi_{1-x}Co_xO_{4\pm\delta}$ compounds having low activation energy (in the range 0.04–0.09) can be used as mixed ionic–electronic conductors (MIECs) [46].

The room temperature resistivity (ρ_{RT}) values as a function of cobalt content x are presented in Fig. 10. As it can be observed, the ρ_{RT} of the samples is constant up to $x \approx 0.5$, then increases rapidly with x. It is significant to note that room temperature resistivity exhibits an increase each time x increases, which is different from the evolution in the formal valence of cobalt. Referring to Brian et al. [18], the half-filled $\sigma^*_{x^2-y^2}$ band is responsible for the metallic behavior of $NdSrNiO_4$ compound. In the present research, when substituting Ni^{3+} for Co^{2+}/Co^{3+} (electronic configuration $t_{2g}^6 d_{z^2}^1 d_{x^2-y^2}^0$/ $t_{2g}^6 d_{z^2}^0 d_{x^2-y^2}^0$), the half-filled $\sigma^*_{x^2-y^2}$ band changes gradually to a half-filled $\sigma^*_{z^2}$ band due to the presence of Co^{2+} cation. On the

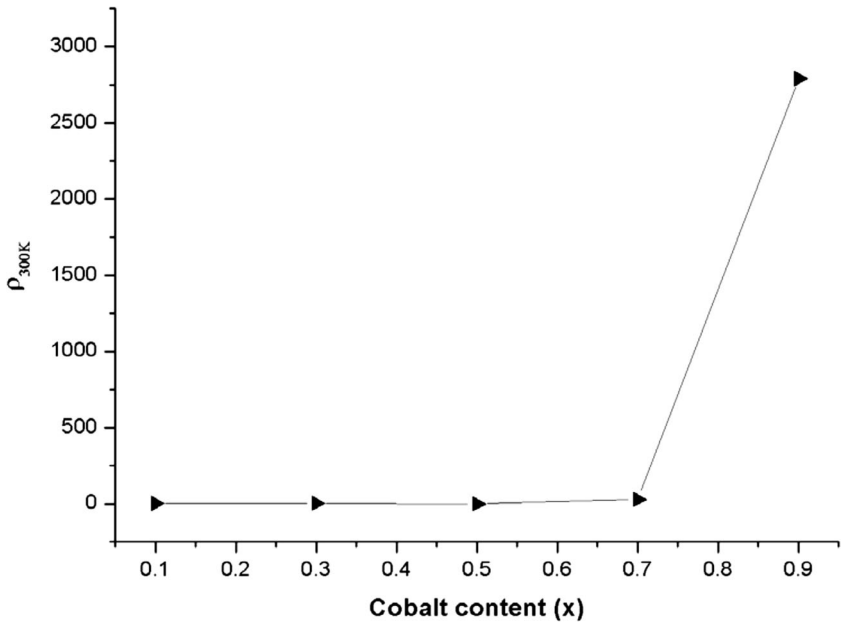

Fig. 10 The room temperature resistivity as a function of cobalt content

other side, when we have compositions corresponding to a higher percentage of cobalt than that of nickel ($x > 0.5$), the resistivity increases remarkably with the incorporation of the diamagnetic Co^{3+} (t_{2g}^6) cation.

On the basis of the electrical resistivity ($\rho_{300K} = 0.058\ \Omega$ cm in bulk form) and the structural and microstructural characteristics of the $NdSrNi_{0.5}Co_{0.5}O_{4\pm\delta}$ material, and at least, it can be successfully deposited in thin film and used as a bottom electrode suitable for the epitaxial regrowth of functional ferroelectric-based parallel plate capacitors. Our material has great potential for other applications as an electrode in solid oxide fuel cells (SOFCs) operating at intermediate temperatures.

Conclusion

Cobalt can be successfully substituted for nickel in the parent compound $NdSrNiO_4$. Refinements of X-ray diffraction data for all compositions (x = 0.1, 0.3, 0.5, 0.7, 0.9) show that these phases crystallize in the tetragonal K_2NiF_4-type structure (I4/mmm space group with z = 2). Oxygen content deduced from thermogravimetric analysis (TGA) under reducing atmosphere displays substantial deviations from the ideal values after the incorporation of cobalt in the structure. These oxygen vacancies are the possible ionic charge carriers. The a and c unit cell parameters values exhibit certain variations with increasing cobalt content. This behavior is deduced from Jahn–Teller distortions as well as the presence of the mixed valence of Co^{2+}/Co^{3+} ions. Bond valence calculations show that cobalt has an oxidation state between two and three. The GII of $NdSrNi_{1-x}Co_xO_{4-\delta}$ ($0.1 \le x \le 0.9$) compounds indicates that the crystal structure becomes more stable when we substitute nickel for cobalt. The transport mechanism in $NdSrNi_{1-x}Co_xO_{4-\delta}$ ($0.1 \le x \le 0.9$) solid solution has been investigated and shows an adiabatic small polaron hopping model. Departing the activation energy that has been undertaken, it is possible to conclude that $NdSrNi_{1-x}Co_xO_{4\pm\delta}$ (x = 0.1, 0.3, and 0.5) compounds are semiconductors with low activation energy. This paper has clearly demonstrated that the composition $NdSrNi_{0.5}Co_{0.5}O_{4\pm\delta}$ exhibits the most interesting physical properties: maximum conductivity at room temperature $\sigma = 17.24\ \Omega^{-1}\ cm^{-1}$ is coinciding with minimum activation energy (E_a = 0.05 eV). These findings are of direct practical relevance in SOFCs and plate capacitors (bottom electrode).

Acknowledgements The authors express sincere thanks to S. PAOFAI and J. ROCHERULLE for their technical assistance as well as their contribution in TGA. Collective and individual acknowledgements are also owed to T. GUIZOUARN for his constant support in terms of electrical measurements.

References

1. Hohlwein D, Hoser A, Sonntag R, Prandl W, Schafer W, Kiemel R, Kemmler-Sack S, Hewat AW (1989) Structural changes in superconducting $La_{1.8}Sr_{0.2}CuO_4$ by alloying copper with cobalt. Phys B Condens Matter 156-157:893–896
2. Zaghrioui M, Giovannelli F, Poirot N, Brouri D, Laffez I (2004) Anomalies in magnetic susceptibility of nonstoichiometric $Nd_2NiO_{4+\delta}$ (δ = 0.049, 0.065, 0.077, 0.234). J Solid State Chem 177:3351–3358
3. Matsuura T, Tabuchi J, Mizusaki J, Yamauchi S, Fueki K (1988) Electrical properties of $La_{2-x}Sr_xCoO_4$—II: models and analysis of the relationship between cobalt 3*d* electron state and structural, electrical and magnetic properties. J Phys Chem Solids 49:1409–1418
4. Luo L, Shao G, Duan Z (2005) Catalytic oxidation properties and characterization of $LaSrCo_{0.9}B'_{0.1}O_4$ (B′ = Mn, Fe, Ni, Cu) mixed oxides. Turkish J Chem 29:597–605
5. Iguchi E, Nakatsugawa H, Futakuchi K (1998) Polaronic conduction in $La_{2-x}Sr_xCoO_4$ ($0.25 \le x \le 1.10$) below room temperature. J Solid State Chem 139:176–184
6. Ferchaud C, Grenier JC, Zhang-Steenwinkel Y, Van Tuel MMA, Van Berkel FPF, Bassat JM (2011) High performance praseodymium nickelate oxide cathode for low temperature solid oxide fuel cell. J Power Sources 196:1872–1879
7. Chauveau F, Mougin J, Mauvy F, Bassat JM, Grenier JC (2011) Development and operation of alternative oxygen electrode materials for hydrogen production by high temperature steam electrolysis. Int J Hydrog Energy 36:7785–7790
8. Grimaud A, Mauvy F, Bassat JM, Fourcade S, Marrony M, Grenier JC (2012) Hydration and transport properties of the $Pr_{2-x}Sr_xNiO_{4+\delta}$ compounds as H^+-SOFC cathodes. J Mater Chem 22:16017–16025
9. Patrakeev MV, Naumovich EN, Kharton VV, Yaremchenko AA, Tsipis EV, Nunez P, Frade JR (2005) Oxygen nonstoichiometry and electron-hole transport in $La_2Ni_{0.9}Co_{0.1}O_{4+\delta}$. J. Solid State Ionics 176:179–188
10. Vashook VV, Ullmann H, Olshevskaya OP, Kulik VP, Lukashevich VE, Kokhanovskij LV (2000) Composition and electrical conductivity of some cobaltates of the type $La_{2-x}Sr_xCoO_{4.5-x/2\pm\delta}$. J Solid State Ionics 138:99–104
11. Moritomo Y, Higashi K, Matsuda K, Nakamura A (1997) Spin-state transition in layered perovskite cobalt oxides: $La_{2-x}Sr_xCoO_4$ ($0.4 \leqslant x \leqslant 1.0$). Phys Rev B 55:14725
12. Shimada Y, Miyasaka S, Kumai R, Tokura Y (2006) Semiconducting ferromagnetic states in $La_{1-x}Sr_{1+x}CoO_4$. Phys Rev B 73:134424
13. Kharton VV, Yaremchenko AA, Shaula AL, Patrakeev MV, Naumovich EN, Logvinovich DI, Frade JR, Marques FMB (2004) Transport properties and stability of Ni-containing mixed conductors with perovskite and K_2NiF_4-type structure. J Solid State Chem 177:26–37
14. Huang S, Ruan K, Lv Z, Wu H, Pang Z, Cao L, Li X (2006) Evidence for spin-glass states and Griffiths singularities in $Nd_{0.75}Sr_{1.25}CoO_4$. J Phys Condens Matter 18:7135–7144
15. Huang S, Ruan K, Lv Z, Zhuang L, Wei P, Wu H, Li M, Zhang J, Chai Y, Yang H, Cao L, Li X (2006) Magnetic and transport properties in layered $Nd_{1-x}Sr_{1+x}CoO_4$. Phys rev B 73:94431
16. Grandjean D, Weller MT (1993) Structure and oxygen stoichiometry in complex neodymium strontium cobalt copper oxides: $[NdSrCo_{1-x}Cu_xO_{4-y}]$. J Mat Res Bull 28:685–692
17. Chaker H, Roisnel T, Potel M, Ben Hassen R (2004) Structural and electrical changes in $NdSrNiO_{4-\delta}$ by substitute nickel with copper. J Solid State Chem 177:4067–4072

18. Arbuckle BW, Ramanujachary KV, Zhang Z, Greenblatt M (1990) Investigations on the structural, electrical, and magnetic properties of $Nd_{2-x}Sr_xNiO_{4+\delta}$. J Solid State Chem 88:278–290
19. Chaker H, Députier S, Guizouarn T, Ben Hassen R, Perrin A, Guilloux-Viry M (2009) $NdSrNi_{0.8}Cu_{0.2}O_{4-\delta}$ thin films epitaxially grown by pulsed laser deposition on $LaAlO_3$ and $SrTiO_3$: a potential electrode for epitaxial regrowth of perovskite structure-based oxides. J Cryst Growth 311:2746–2752
20. Chaker H, Roisnel T, Cador O, Amami M, Ben Hassen R (2006) Neutron powder diffraction studies of $NdSrNi_{1-x}Cu_xO_{4-\delta}$, $0 \le x \le 1$ and magnetic properties. J Solid State Sci 8:142–148
21. Chaker H, Roisnel T, Ceretti M, Ben Hassen R (2007) The synthesis, structural characterization and magnetic properties of compounds in the Ln_2O_3-SrO-NiO-CuO system for Ln = La, Nd, Gd, Dy, Ho and Er. J Alloys Comp 431:16–22
22. Hamdi S, Ouni S, Chaker H, Ben Hassen R (2012) Synthesis, structural and electrical characterizations of $Er_{0.33}Sr_{1.67}Ni_{0.8}Cu_{0.2}O_{4-\delta}$. J Powder Diffract 27:252–255
23. Hamdi S, Ouni S, Chaker H, Rohlicek J, Ben Hassen R (2011) Synthesis, structural and electrical characterizations of $DySr_5Ni_{2.4}Cu_{0.6}O_{12-\delta}$. J Solid State Chem 184(11):2897–2901
24. Chaker H, Roisnel T, Ceretti M, Ben Hassen R (2010) Rietveld refinement of X-ray powder data and bond valence calculations of $NdSrNi_{0.5}Cr_{0.5}O_{4-\delta}$ compound. J Powder Diffract 25:241–246
25. Jammali M, Chaker H, Cherif K, Ben Hassen R (2010) Investigation on the structural and electrical properties of $NdSrNi_{1-x}Cr_xO_{4+\delta}$ ($0.1 \le x \le 0.9$) system. J Solid State Chem 183:1194–1199
26. Jammali M, Ben Hassen R, Rohlicek J (2012) Structural and electrical properties of $Nd_{1.7}Ba_{0.3}Ni_{0.9}Cr_{0.1}O_{4+\delta}$ compound. J Powder Diffract 27:184–188
27. Rodriguez-Carvajal J (2001) Recent developments of the program FULLPROF. IUCr-CPD. News Lett 26:12
28. Van der Pauw LJ (1958) A method of measuring specific resistivity and hall effect of discs of arbitrary shape. Philips Res Rep 13:1–9
29. Shannon RD (1976) Revised effective ionic radii and systematic studies of interatomic distances in halides and chalcogenides. Acta Crystallogr Sect A 32:751–767
30. Goldschmidt VM, Oslo A (1926) I Mater Nat 2:7
31. Ganguly P, Rao CN (1984) Crystal chemistry and magnetic properties of layered metal oxides possessing the K_2NiF_4 or related structures. J Solid State Chem 53:193–216
32. Takeda Y, Nishijima M, Imanishi N, Kanno R, Yamamoto O, Takano M (1992) Crystal chemistry and transport properties of $Nd_{2-x}A_xNiO_4$ (A = Ca, Sr, or Ba, $0 \le x \le 1.4$). J Solid State Chem 96:72–83
33. Altermalt D, Brown ID (1985) The Automatic Searching for Chemical Bonds in Inorganic Crystal Structures. Acta Cryst B 41: 240–244
34. Salinas-Sánchez A, García-Muñoz JL, Rodríguez-Carvajal J, Saez-Puche R, Martínez JL (1992) Structural characterization of R_2BaCuO_5 (R = Y, Lu, Yb, Tm, Er, Ho, Dy, Gd, Eu and Sm) oxides by X-ray and neutron diffraction. J Solid State Chem 100:201–211
35. Sánchez-Andújar M, Señarís-Rodríguez MA (2004) Synthesis, structure and microstructure of the layered compounds $Ln_{1-x}Sr_{1+x}CoO_4$ (Ln: La, Nd and Gd). J Solid State Sci 6:21–27
36. Brown ID, Altermatt D (1985) Bond-valence parameters obtained from a systematic analysis of the inorganic crystal structure database. Acta Crystallogr B41:244–247
37. Wood RM, Palenik GJ (1998) Bond valence sums in coordination chemistry. A simple method for calculating the oxidation state of cobalt in complexes containing only Co−O bonds. Inorg Chem 37: 4149–4151
38. Rodriguez-Carvajal J Private communication
39. Lewandowski JT, Beyerlein RA, Longo JM, Mccauley RA (1986) Nonstoichiometric K_2NiF_4-type phases in the lanthanum-cobalt-oxygen system. J Amer Ceram Soc 69:699–703
40. Chaikin PM, Beni G (1976) Thermopower in the correlated hopping regime. Phys Rev B 13:647–651
41. Mott N (1993) Conduction in non-crystalline materials. Clarendon, Oxford, pp 17–23
42. Laiho R, Lisunov KG, Lähderanta E, Stamov VN, Zakhvalinskii VS (2001) Variable range hopping conductivity in $La_{1-x}Ca_xMnO_3$. J Phys Condens Matter 13:1233–1246
43. Ang R, Sun YP, Luo X, Hao CY, Song WH (2008) Studies of structural, magnetic, electrical and thermal properties in layered perovskite cobaltite $SrLnCoO_4$ (Ln = La, Ce, Pr, Nd, Eu, Gd and Tb). J Phys D App Phys 41(4). doi:10.1088/0022-3727/41/4/045404
44. Taguchi H, Nakade K, Hirota K (2007) Synthesis and characterization of K_2NiF_4-type $CaLnCoO_4$ (Ln = Sm and Gd). Mater Res Bull 42:649–656
45. Taguchi H, Hirata K, Kido H, Takeda Y, Kato M, Hirota K (2009) Hopping conductivity of distorted K_2NiF_4-type $(Ca_{1+x}Nd_{1-x})CrO_4$. Solid State Sci 11:1222–1225
46. Khandale AP, Bansod MG, Bhoga SS (2015) Improved electrical and electrochemical performance of co-doped $Nd_{1.8}Sr_{0.2}Ni_{1-x}Cu_xO_{4+\delta}$. Solid State Ionics 276:127–135